HighResClimNevada: a high-resolution climatological dataset for a high-altitude region in Southern Spain (Sierra Nevada)

Matilde García-Valdecasas Ojeda[1,2], Feliciano Solano-Farias[1], David Donaire-Montaño[1], Emilio Romero-Jiménez[1], Juan José Rosa-Cánovas[1,2], Yolanda Castro-Díez[1,2], Sonia R. Gámiz-Fortis[1,2], and María Jesús Esteban-Parra[1,2]

[1]Department of Applied Physics, University of Granada, Granada, 18071, Spain
[2]Atmosoheric Physics, Andalusian Inter-University Institute for Earth System Research, Granada, 18071, Spain

Correspondence to: Matilde García-Valdecasas Ojeda (mgvaldecasas@ugr.es)

Abstract. Climate datasets with very high spatiotemporal resolution are essential to assess the impacts of climate change in mountain areas, which are complex systems in which climate is very changeable. However, these regions are characterized by a lack of climatic information, and if any, it is usually short, sparse, or incomplete. This work presents a new series of very high-resolution (1 km) gridded climate datasets for Sierra Nevada (SN), a mountain range classified as a double climate-change hotspot, as it is a semi-arid mountain range in the Mediterranean area that is particularly vulnerable to climate change. The database, called HighResClimNevada, consists of a set of climate data derived from a climate simulation using the Weather Research and Forecasting (WRF) model for the period from 1991 to 2022 and forced with the ERA5 reanalysis. HighResClimNevada provides hourly/daily primary climate variables (i.e., near-surface temperature, precipitation, near-surface relative humidity, surface pressure, surface net radiation, and wind speed), but also bioclimatic variables, extremes indices from the Expert Team of Climate Change Detection and Indices (ETCCDI), and precipitation-hour indicators, which were postprocessed using aggregated temperature and precipitation values from primary climate variables. To evaluate the database performance, HighResClimNevada temperature and precipitation values were compared with reference datasets from different sources. In general, HighResClimNevada captures reasonably well the spatiotemporal variability of raw temperature but also bioclimatic variables and extreme indices in SN. It displays comparable behavior to other climatic products but with a greater level of detail due to its higher spatial resolution. For precipitation, variable, more uncertain and difficult to characterize, HighResClimNevada exhibits a higher amount of precipitation when compared to station-based, coarse satellite-based, and reanalysis-based products. However, these latter present problems in characterizing precipitation in high mountain regions probably due to the scarcity of data in areas with high spatiotemporal variability, such as SN. The precipitation from HighResClimNevada is comparable to other climatic products like CHIRPS or CERRA-Land, which captures better the spatiotemporal variability in this region. These findings, therefore, suggest HighResClimNevada as a valuable long-term climate tool for a variety of applications, including land management, hydrometeorological research, flora and fauna phenology, and risk assessment. The reported datasets are freely available for download via Zenodo platform (Garcia-Valdecasas Ojeda et al., 2025, https://doi.org/10.5281/zenodo.14883471).

1. Introduction

Mountain areas are particularly vulnerable to climate change due to several causes. On the one hand, these regions are characterized by extreme climatic conditions, forcing species of flora and animals to adapt to this environment. Consequently, mountains are rich in biodiversity, including endemic species. However, this fact makes these regions vulnerable, as species that are high-altitude specialists may be less resilient under a changing climate. As a result, if the warming rate continues, natural ecosystems may suffer catastrophic consequences due to a decrease in biodiversity (La Sorte and Jetz, 2010) or a reduction of the habitats for many species (Parmesan, 2006). For example, the rising temperatures caused by climate change are leading to an upward migration of flora and fauna species (Parmesan, 2006). Subsequently, mountain biodiversity, particularly endemic species and those with limited dispersal capacity (Viterbi et al., 2013), is being affected by the emergence of invasive species. On the other hand, high altitude areas play a key role in providing water resources to ecosystems and humans (Viviroli et al., 2020). These regions are, however, suffering unprecedented water stress as a result of increasing economic and demographic expansion (Beniston, 2003). This is particularly true over Mediterranean regions, where mountains serve as the main source of fresh water for downstream communities (the so-called water tower), who rely heavily on it during the late spring and summer (Polo et al., 2020). Moreover, mountains are undergoing rapid environmental change (Beniston et al., 2018; Gobiet et al., 2014), caused, among other factors, by the substantial increasing temperature trend that occurred in these areas. Many studies have reported elevation-dependent warming (EDW) due to different climate mechanism, such as the snow-albedo feedback (Pepin et al., 2019, 2022; Rangwala and Miller, 2012). Specifically, an increasing temperature trend (around 0.13 ºC per decade) has been found over European mountains such as the Alps since the 19th century (Begert and Frei, 2018), which has become more pronounced, especially after the 1980s, with a warming rate of 0.5 ºC per decade (Nigrelli and Chiarle, 2023). This increased trend has also been found in southern Europe, such as the Pyrenees (0.17 ºC per decade) and the Sierra Nevada (0.13 ºC per decade), where increasing patterns are more generalized for the minima (Esteban-Parra et al., 2022; Sigro et al., 2024). In the latter area, moreover, the drying trend in annual and winter precipitations (Esteban-Parra et al., 2022) is becoming a threat to the ecosystems that inhabit this region.

To understand the causes of many fundamental questions and applications in environmental research and ecology in a changing climate over high mountains, long and temporally consistent climate data with high resolution in space and time is critical (Hartmann et al., 2000). This is even more relevant in high mountains, where limitations in measurement equipment or sensor maintenance make obtaining adequate climate records extremely challenging. As a result, climate information in these regions is usually short, sparse, or incomplete, and therefore, how the climate is changing in these regions remains uncertain. In this regard, regional climate models (RCMs) have proven to be useful tools as they can provide climate information regularly in space and time, allowing the development of consistent long-term climate data in regions with difficult access. This is particularly true when working with an RCM with a high resolution ($\Delta x \leq 4$ km). At these spatial resolutions, deep convection can be explicitly resolved by the RCM instead of being parameterized, a reason why RCMs at km-scale resolution are known as convection-permitting models (CPMs) or convection-permitting RCMs (CPRCMs). This fact implies a significantly

65   enhanced representation of orography and land-surface information. As a result, CPRCMs can better capture orographic precipitation and extreme rainfall events, as well as soil-atmosphere and cloud-radiation feedbacks and mountain snowpack (Coppola et al., 2020; Halladay et al., 2024; Lucas-Picher et al., 2024; Prein et al., 2015, 2017, 2020; Sangelantoni et al., 2022, among others), leading to a more realistic climate information.

This study describes a new series of 32-year high-resolution climate datasets for Sierra Nevada (SN), a Mediterranean
70   mountain range in the Southern Iberian Peninsula (IP) that constitutes a double hotspot region. These datasets, called HighResClimNevada, provide primary climatic variables, bioclimatic variables, and extremes indices in a region with scarce climatic information with quality due to the difficulty of access. Furthermore, HighResClimNevada provides information at unprecedented spatial resolution in this region which is useful for studies focusing on the impacts of climate change on botany, ecology, and other disciplines. HighResClimNevada, derived from climate modeling using a CPM, is available for the period
75   from January 1991 to December 2022.

This paper is structured as follows: Section 2 describes the model configuration for the development of HighResClimNevada, data used as a reference for the evaluation of HighResClimNevada, and variables provided by HighResClimNevada. Section 3 displays and discusses the results of the HighResClimNevada evaluation, Section 4 describes the data and code availability, and Section 5 summarizes and concludes the main findings of this work.

 1.   Methods

2.1.   Study region

SN, located in the Baetic System (latitudes 36.93ºN to 37.20ºN and longitudes 3.53ºW to 2.65ºW), is the southernmost mountain range on the European continent. It houses some of the highest peaks in the IP, including Mulhacén (3479 m) and Veleta (3396 m) (Oliva et al., 2022). SN is a clear example of semi-arid high mountains being considered a double hotspot region where Mediterranean and Alpine climates cohabit about 40 km apart (Polo et al., 2019). Due to its singular conditions, it is home to many endemic plant and animal species, being considered one of the most important European hotspots for biodiversity (Blanca et al., 1998), and being a good candidate as a global change observatory. For these reasons, it was designated a Biosphere Reserve by UNESCO in 1986, Natural Park in 1989, and National Park in 1999.
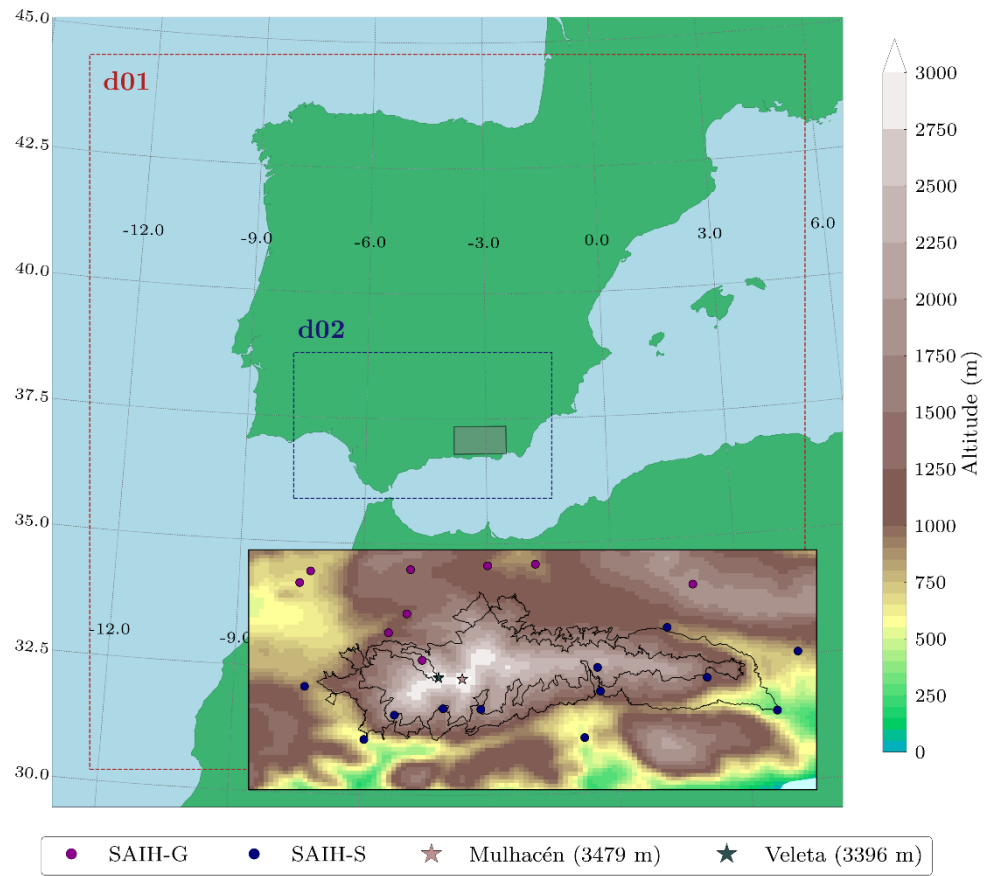
Figure 1: WRF domain configuration with two one-way domains: the parent domain (d01), which covers the Iberian Peninsula (IP) with 5 km spatial resolution, and the inner domain (d02), which spans the Andalusia region with 1 km spatial resolution. The area covered by HighResClimNevada is depicted in the inner figure at the bottom right, including the boundaries of both the Natural and National Parks of Sierra Nevada (black contours). The shading colors in this subfigure denote the elevation stated in meters above mean sea level, while the dots represent the locations of stations from the HidroSur automatic Hydrological Information System (SAIH-S) and the Guadalquivir automatic Hydrological Information System (SAIH-G).

2.2.   Climate model

HighResClimNevada has been developed using the Weather Research and Forecasting Model (WRF) version 4.3.3 (Skamarock et al., 2021). This model was chosen for its ability to accurately characterize climate variables such as precipitation in complex topographical regions as the IP, particularly for spatial resolutions of a few kilometers (i.e., grid-spacing < 4 km, convection-permitting mode). To do that, a one-way double-nested configuration with a 5:1 nesting ratio (Fig. 1) was chosen: a parent domain (d01), which spans the whole IP with 5 km spatial resolution, and a nested domain (d02) covering SN with 1 km spatial resolution. In order to preserve a resolution step lower than 12 (Denis et al., 2003), we adopt a multi-nest approach. This avoids the necessity of a large spin-up zone in our simulation. We have followed, therefore, the recommendation of authors such as Matter et al. (2016), who pointed out double-nested configurations in a trade-off between quality and computational cost. On the other hand, the use of a one-way strategy was based on previous studies such as Messmer et al. (2021), who, in addition, found that a two-way strategy affects the representation of the domain when convection is disabled. The Lambert projection was used with the center at 37.65ºN, 3.97ºW, and with 320 x 320 and 576 x 326 grid points in the west-east and south-north directions for d01 and d02, respectively. In the vertical, both domains were configured using 46 hybrid levels, with the top set to 50 hPa.

WRF was updated every six hours using the fifth-generation European ReAnalysis (ERA5, Hersbach et al., 2020), the latest reanalysis product from the European Centre for Medium-Range Weather Forecasts, which has been shown to be effective for regional climate downscaling. Although ERA5 provides hourly data, we opted for a six-hour update frequency to allow the model a certain degree of free evolution (González-Rojí et al., 2022). Additionally, using hourly data for a 32-year climate simulation would be impractical due to the high storage and computational demands. To complete the entire period (1991-2022), the simulation was divided into 11-year runs, with the first year of each simulation being the spin-up of the model. This spin-up period was selected to balance the impact on simulations when a short spin-up period is used and the computational cost of CPM simulations. In this regard, a study conducted by Jerez et al. (2020) found that for atmospheric variables such as precipitation and temperature, a relatively short spin-up time (~ 1 week) is required. However, soil variables need longer periods to reach such an equilibrium, and it depends on the initial soil moisture conditions and soil depth, among others (Khodayar et al., 2015). In this context and considering the trade-off between suitability and computational resources, as well as the fact that this study uses ERA5 data as LBCs, one year as spin-up was finally used.

For the selection of physical schemes, we applied the configuration suggested by Solano-Farías et al. (2024). This configuration was achieved by performing a sensitivity study resulting from combining different microphysics and convection schemes in the parent domain (d01), i.e., convection was switched off in the inner domain (d02) for all experiments. As a result, 12 WRF simulations of 1 year length were completed and compared with different reference datasets in terms of precipitation and maximum and minimum temperatures. From that work, the authors concluded that the combination of parameterizations composed by the WRF single-model 7-class (WSM7, Bae et al., 2019), Grell-Freitas (Grell and Freitas, 2014) for convection in the parent domain (d01), the Community Atmosphere Model 3.0 (CAM3.0, Collins et al., 2004) for both long- and short-

wave radiation, the Asymmetric Convective Model version 2 (ACM2, Pleim, 2007) for planetary boundary layer (PBL), and the multiparametric Noah (NOAH-MP, Yang et al., 2011) land surface model (LSM) leads to an adequate characterization of climate conditions over Andalusia. A summary of the model configuration can be seen in Table 1.

Table 1: Main characteristics of the WRF model configuration applied to create the HighResClimNevada data.

	Parent domain (d01)	Nested domain (d02)
Regional climate model		
WRF-ARW v4.3.3 (Skamarock et al., 2021)		
Lateral Boundary Conditions		
ERA5 Reanalysis (Hersbach et al., 2023) every 6-hours		
Domain configuration		
Nesting strategy:	One-way	
Spatial resolution:	5 km	1 km
Coverage:	Iberian Peninsula	Andalusia
Dimensions (grid points):	320 x 320	576 x 326
Vertical coordinate system:	Hybrid	Hybrid
Number of vertical levels:	46	46
Model top pressure:	50 hPa	50 hPa
Time step:	30 seconds	6 seconds
Parameterization schemes		
Land surface model:	Noah MP (Yang et al., 2011)	Noah MP (Yang et al., 2011)
Planetary boundary layer:	ACM2 (Pleim et al., 2007)	ACM2 (Pleim et al., 2007)
Convection:	GF (Grell and Freitas, 2014)	OFF
Microphysics:	WSM7 (Bae et al., 2019)	WSM7 (Bae et al., 2019)
Long-wave radiation:	CAM3 (Collins et al., 2004)	CAM3 (Collins et al., 2004)
Short-wave radiation:	CAM3 (Collins et al., 2004)	CAM3 (Collins et al., 2004)
Atmospheric surface layer:	Revised MM5 (Jiménez et al., 2012)	Revised MM5 (Jiménez et al., 2012)
Spin-up time:	1-year	1-year

2.3. Reference datasets

Observational datasets, although valuable, are not error-free, particularly in mountainous regions, where uncertainties tend to be more pronounced (Prein and Gobiet, 2017). Thus, daily values of precipitation (pr) and maximum, mean, and minimum temperature (tasmax, tasmean, and tasmin, respectively) were used from different sources (Table 2) to evaluate the HighResClimNevada performance, avoiding drawing incorrect conclusions due to observational uncertainties.

Satellite-based precipitation estimations were considered as a source of precipitation information. The United States Global Precipitation Measurement (GPM) Team and the National Aeronautics and Space Administration (NASA) of United States developed the Integrated Multi-SatellitE Retrievals (IMERG) for GPM version 6 (Huffman et al., 2019, 2020). This half-hourly multi-satellite-based product provides precipitation estimates for almost the entire planet with a spatial resolution of 0.1º and for a period from 2000 to 2021. Among the different versions, IMERG Final run was selected, which is calibrated at a monthly scale using the 1º x 1º Global Precipitation Climatology Centre (GPCC) monthly monitoring product. On the other

hand, the Satellite Precipitation Climate Prediction Center morphing method (CMORPH, Joyce et al., 2004) is a high-quality,

145 high-resolution (~ 8 km of spatial resolution and a half-hourly time frequency) dataset developed by the National Oceanic and Atmospheric Administration (NOAA) of the United States. CMORPH, which is derived from low orbiter satellite microwave measurements, is available for the period 1998 to near present for the latitudinal bands from 60 ºN to 60 ºS. The Climate Hazards group InfraRed Precipitation with Stations data (CHIRPS, Funk et al., 2015) includes gridded products that provide precipitation estimates for latitudinal bands between 50ºS and 50ºN. This data combines satellite precipitation data from NASA

150 and NOAA with in-situ station data from public and commercial archives. The global daily CHIRPS v2 with 0.05º spatial resolution, available since 1981, was used.

Additionally, gridded station-based products were used. On the one hand, meteorological gridded products developed by Peral García et al. (2017) version 2 (referred to as ROCIO_IBEB) were used. These daily datasets are the result of interpolating high-quality observational time series from the Spanish Meteorological Agency's (AEMET) National Bank of Climatological

155 Data. ROCIO_IBEB provides precipitation and extreme temperature (maximum and minimum) values for Peninsular Spain and Balearic Islands at a 5 km spatial resolution from 1951 to 2022. On the other hand, a monthly precipitation dataset (UGR-SNGrid) developed by the Atmospheric Physics Group at the University of Granada (Romero-Jiménez et al., 2024) was also employed. UGR-SNGrid is a gridded dataset covering the SN Natural Park and its surroundings from 1990 to 2020, with a spatial resolution of 200 meters. For its development, precipitation records from the ClimaNevada database

160 (https://climanevada.obsnev.es/) and the automated Hydrological Information System (SAIH) network were subjected to rigorous quality control before being spatially interpolated using the R package RegRAIN version 0.1.0 (Alzate Velásquez et al., 2017). Based on the Regionalisierte Niederschlage (REGNIE) method (Rauthe et al., 2013), RegRAIN combines multiple linear regression considering orographical factors such as location, slope, elevation, and inverse distance weighting. The orographical factors were obtained from a digital elevation model and monthly regressions are calculated using precipitation

165 time series from stations. More details about this methodology can be found in in Romero-Jiménez et al. (2023).

Reanalysis data were employed as an additional source of information that would complement the sparse station network in this area. On the one hand, the global ERA5-Land reanalysis (Muñoz-Sabater et al., 2021) provides climatic and land-related variables with a 9 km spatial and hourly timestep. It was developed using ERA5 as atmospheric forcing and is available from January 1950 to the near present. Additionally, the Copernicus European Regional ReAnalysis products (CERRA and CERRA-

170 Land) were used. Both regional products are high-resolution reanalysis developed using dynamical downscaling methods. The CERRA reanalysis (Schimanke et al., 2021) employs ARMONIE-ALADIN as limited-area numerical weather model, which is driven by ERA5, and the CERRA system to assimilate a dense network of in situ observations and satellite information. CERRA-Land (Verrelle et al., 2022), on the other hand, employs the land surface model SURFEX v8.1, which is run offline forced using 3-hourly CERRA atmospheric variables and the daily surface precipitation from the MESCAN system. CERRA

175 and CERRA-Land have the same integration domain (e.g., orography, coverage, etc.) and provide surface variables with 5.5 km spatial resolution from 1984 to 2021.

Precipitation and temperature data from weather stations have also been used for the evaluation of HighResClimNevada. Hourly data from the Automatic Hydrological Information System (SAIH) HidroSur (SAIH-S, http://www.redhidrosurmedioambiente.es) and Guadalquivir (SAIH-G, https://www.chguadalquivir.es), which are networks

180 of high-quality stations with hourly precipitation and temperature data from 1997 and 2001, respectively, to the present, were used. To preserve as much quality climate data as possible, SAIH-G and SAIH-S time series with at least 85% of records for a period of at least 19 years within the study period were used. For precipitation, the SAIH-S and SAIH-G stations were 19 and 13, respectively. For temperature, however, two stations were selected and only from SAIH-S.

All these databases were downloaded at their native temporal resolution for the time period covered by HighResClimNevada

185 and then aggregated to daily scale in cases where the resolution differed.

Table 2: Precipitation and temperature datasets used as reference in the evaluation of HighResClimNevada, classified according to their origin. Each reference database is identified by ist name. Additionally, their spatial coverage, resolution (gridded products) or number of stations (punctual stations), temporal aggregation, available period (used) and studied variables are also shown. Pr, tasmax, tasmean, and tasmin denote daily accumulated precipitation and maximum, mean, and minimum temperatures,

190 **respectively. Hourly mean temperature is denoted as ta in order to differentiate it from daily values.**

Name	Coverage (resolution or number or stations for pr (ta))	Temporal frequency	Available (analysis) period	Variable
Gridded dataset developed with in-situ stations				
ROCIO_IBEB	Peninsular Spain and Balearic Islands (0.05º)	daily	1951-2022 (1991-2022)	pr, tasmax, tasmin
UGR-SNGrid	Sierra Nevada (200 m)	monthly	1990-2020 (1991-2020)	pr
Satellite-derived gridded products				
CMORPH	Latitudinal bands from 60ºN and 60º S (8 km)	half-hourly	1998-present (1998-2022)	pr
GPM IMERG	Quasi global (0.1º)	half-hourly	2000-2021 (2001-2020)	pr
CHIRPS	Latitudinal bands from 50ºN to 50º S (0.05º)	daily	1981-present (1991-2022)	pr
Reanalysis gridded products				
ERA5-Land	Global (~9km)	1-hourly	1950-present (1991-2022)	pr, ta
CERRA	Europe (5.5 km)	3-hourly	1984-2021 (1991-2021)	ta
CERRA-Land	Europe (5.5 km)	daily	1984-2021 (1991-2021)	pr
Punctual in-situ stations				
Automatic Hydrological Information System (SAIH) stations	Guadalquivir (SAIH-G, 9) and southern (SAIH-S, 13 (2)) hydrological basins	1-hourly	SAIH-G: 2001-present (2001-2022), SAIH-S: 1997-present (1997-2022)	pr, ta

2.4. Climate variables in HighResClimNevada: format and file organization

HighResClimNevada has been structured in netCDF files that contain 3D climate fields (time x latitude x longitude) covering longitudes from 3.85ºW to 2.40ºW and latitudes from 36.50ºN to 37.50ºN (see Fig. 1). These data are provided in the original Lambert grids for a period from January 1991 to December 2022. All files also provide a 2D mesh with the altitude (z) at sea level expressed in meters above the mean sea level and includes variables over land. The database is divided into (1) primary climate variables, (2) bioclimatic variables, (3) extreme ETCCDI climate indices, and (4) precipitation-hour extreme variables.

2.4.4. Primary climate variables

- Near-surface temperature (ta, ºC): temperature plays a crucial role in ecosystem functions being variables commonly used to describe the climate in a region. Near surface (2 m) temperature was obtained from raw simulation outputs with a 10-minute temporal resolution. Then, hourly (ta) and daily mean of the maximum (tasmax), mean (tasmean), and minimum (tasmin) temperatures were calculated based on these values.

- Precipitation (pr, kg m^{-2}): the accumulated precipitation amounts were obtained from raw 10-minute WRF outputs. As for temperature, these values were then aggregated on hourly and daily scales to be part of the HighResClimNevada datasets.

- Near-surface relative humidity (hur, %): changes in humidity over land also have important implications on ecosystems. 3-hourly outputs of water vapor mixing ratio at 2 m (r, kg*kg^{-1}), near surface temperature (ta, ºC), and surface pressure (ps, hPa) provided by WRF were used to estimate hur using Equations 1, 2, and 3.

$$e_s = 6.11 \ 10^{\frac{7.5(ta - 273.15)}{(ta - 273.15) + 237.3}} \tag{1}$$

$$r_s = \frac{0.622 e_s}{ps - e_s} \tag{2}$$

$$hur = \frac{r}{r_s} \times 100 \tag{3}$$

where e_s is the water vapor pressure and r_s is the saturated mixing ratio in kg*kg^1. Then, 3-hourly hur were used to estimate the daily averages.

- Surface pressure (ps, Pa): atmospheric pressure was averaged at a daily scale using the corresponding 3-hourly surface pressure from WRF outputs.

- Surface net radiation (net_radiation, W m^{-2}): it is the radiant energy available at the surface to perform work inside the ecosystem and is critical for maintaining biological and physical processes. Surface net radiation is calculated as the balance between the absorbed, reflected, and emitted energy by the Earth's surface, using 3-hourly outputs and following Equation 4.

$$net\_radiation = \left(R_S\downarrow - R_S\uparrow\right) + \left(R_L\downarrow - R_L\uparrow\right) \tag{4}$$

215   where $R_s\downarrow$ (W m^{-2}) is the incoming solar radiation, $R_s\uparrow$ (W m^{-2}), is the proportion of the solar radiation reflected by the surface, $R_L\downarrow$ (W m^{-2}) is the incoming longwave radiation emitted by the atmosphere, and $R_L\uparrow$ (W m^{-2}) is the radiation emitted by the surface.

- Surface wind speed (wind_speed, ms^{-1}): the daily 10-meter wind speed was calculated using 3-hour outputs of U10 (m/s) and V10 (m/s), which are the eastward and northward WRF wind components at 10 m, respectively, using Equation 5.

$$\text{wind\_speed} = \sqrt{U10^2 + V10^2} \qquad (5)$$

220   **2.4.5. Bioclimatic variables**

Based on monthly temperature values and precipitation, bioclimatic variables have been calculated and are available at an annual scale in the HighResClimNevada database. These indices, which describe the ecological and environmental status of ecosystems, were obtained following BIOCLIM WorldClim (Fick and Hijmans, 2017; Hijmans et al., 2005), CHELSA Bioclim (Karger et al., 2017), and CMCC-BioClimInd (Noce et al., 2020) standard definitions. Here, we

225   considered those bioclimatic variables with interest for semi-arid mountains and due to their relevance in agricultural and ecological applications, which are:

- Annual mean temperature (BIO1, ºC): it is calculated for each year by averaging tasmean. Similarly, seasonal values have been considered, with summer (June-July-August, JJA) and winter (December-January-February, DJF) representing the dry/warm and wet/cold seasons, respectively. This variable was also considered for spring (March-

230   April-May, MAM) and autumn (September-October-November, SON) to reflect intermediate seasons. Additionally, the annual average of tasmax (BIO1$_{max}$) and tasmin (BIO1$_{min}$) were calculated as well as the subsequent values for each season.

- Mean Diurnal Range (DTR or BIO2, ºC): it is the difference between the monthly tasmax and tasmin. In this work, BIO2 is referred to as DTR as defined by the ETCCDI as an extreme index of temperature. That is, the daily difference

235   between tasmax and tasmin was calculated to obtain annual means of DTR.

- Isothermality (BIO3, %): it measures the degree of daily temperature fluctuations (BIO2) compared to annual variations throughout extreme months (BIO7) according to Equation 6.

$$BIO3 = \frac{BIO2}{BIO7} \times 100 \qquad (6)$$

- Temperature seasonality (BIO4, ºC): it refers to temperature fluctuations throughout the year. BIO4 is computed as the standard deviation of monthly tasmean, which is obtained using the twelve-monthly values from each year (Noce

240   et al., 2020).

- Maximum temperature of warmest month (BIO5, ºC): it is defined through the monthly means of tasmax. Thus, for each year, the monthly tasmax value of the month with the highest temperature is selected as the maximum temperature of warmest month of that year.

- Minimum temperature of coldest month (BIO6, ºC): similarly to BIO5, monthly means of tasmin are computed throughout the years, and then minimum values for each year are taken as the minimum temperature of coldest month.
- Annual temperature range (BIO7, ºC): it reflects the range of temperatures between the coldest and the warmest months.

$$BIO7 = BIO5 - BIO6 \tag{7}$$

- Mean temperature of wettest quarter (BIO8, ºC): wettest quarters were obtained using as a reference the spatial mean of HighResClimNevada pr in the SN Natural Park. For each year, the 3-month precipitation moving sum is calculated, and the maximum value is determined through its central month. BIO8 is then calculated as the average tasmean of the three consecutive averages starting in the wettest quarters (Noce et al., 2020).
- Mean temperature of driest quarter (BIO9, ºC): similarly to BIO8, driest quarter is obtained for each year looking for the minimum 3-month moving sum determined through its central month. Then, mean temperatures for each year are computed through the 3 consecutive months, starting in the driest quarters.
- Annual precipitation (BIO12, kg m^{-2}): the total amount of precipitation was computed as the average of the annual sum of precipitation. Similarly to temperature, seasonal values (BIO12$_{XXX}$ with XXX being DJF, MAM, JJA, and SON) were obtained.
- Precipitation of wettest month (BIO13, kg m^{-2}): similarly to BIO5, it is computed as the highest monthly sum of precipitation for each year.
- Precipitation seasonality (BIO15, %): it shows the precipitation variations throughout the year and is calculated as the coefficient of variation of monthly values in each year (Equation 8), expressed as percentage.

$$BIO15 = \frac{s_{pr}}{\overline{pr}} \text{ x } 100 \tag{8}$$

where s_{pr} is the annual standard deviation and $\overline{pr}$ is the mean.

- Precipitation of coldest quarter (BIO19, kg m^{-2}): this metric is considered since SN serves as a "water tower" for neighboring regions. Similarly to BIO8 and BIO9, coldest quarters of each year are determined as the lowest temperature of the 3-month moving average from HighResClimNevada. For each year, the precipitation amount is then calculated for the three consecutive months starting in the coldest quarters.

2.4.6. Extreme ETCCDI climate indices

Temperature and precipitation extremes indices from the Expert Team on Climate Change, Detection, and Indices were also calculated. Here, extreme variables with relevance in mountain ecosystems have been considered, and these are:

- Warmest day (TXx, ºC) and coldest night (TNn, ºC): TXx represents the maximum value of tasmax in the warmest month. In the same way, TNn is understood as the lowest value of tasmin in the coldest month.

- Growing season length (GSL, days): the growth season is the time of year when plants grow effectively. According to the ETCCDI, GSL is defined as the number of days per year between the first occurrence of at least 6 days with tasmean > 5 ℃ and the first occurrence (after July 1st) of 6 days with tasmean < 5 °C.
- Icing days (ID, days) and frost days (TNltm2, days): here, mountainous cold extreme patterns are represented by the icing days (annual number of days with tasmax < 0 ℃) and frost days (annual number of days with tasmin < -2 ℃). Note that the original definition for frost day has a threshold of tasmin < 0 ℃, but SN high mountain region, a more extreme threshold must be considered.
- Wet, heavy, and very heavy precipitation days (R1mm, R10mm, and R20mm, expressed in days/year): the frequency of extreme precipitation is explored through the number of days per year with pr > 1 mm (wet days), pr > 10 mm (heavy precipitation days), and pr > 20 mm (very heavy precipitation days).
- Simple daily intensity index (SDII, kg m^{-2}) and wettest pentad (rx5day, expressed in kg m^{-2}): SDII calculates the mean daily pr on wet days (pr >1 mm) for a year and rx5day is the highest total quantity of pr falling on 5 consecutive days. These indices are calculated as a proxy for the magnitude of daily extreme precipitation.
- Consecutive dry days (CDD, expressed in days/year): longest period in a year of consecutive days with less than 1 mm of pr per day. The significance of this index lies in the fact that it serves as a drought indicator, a very relevant aspect in a semiarid region such as SN.

2.4.7. Precipitation-hour extreme indices

Finally, very extreme precipitation events were also considered through precipitation-hour indices, which are:

- Wet-hour frequency (F$_{wet-hour}$, %): percentage of hours per year corresponding to wet hours (pr > 0.1 mm).
- Wet-hour Intensity (I$_{wet-hour}$, kg m^{-2}) refers to the average amount of precipitation in one hour only considering wet hours (pr > 0.1 mm).
- Maximum amount of precipitation in the wettest month (PRWw, kg m^{-2}): following the philosophy of ETCCDI extremes such as TXx or TNn, PRWw is calculated by determining the maximum amount of precipitation in each month, and then the maximum value is determined for each year to obtain the PRWw time series.

Table 3: Bioclimatic variables, ETCCDI, and precipitation-hour extreme indices available in HighResClimNevada. Asterisks (*) indicate self-defined variables, which are based on original bioclimatic variables or ETCCDI indices. The table includes the name of the index, the variables involved, and time aggregation used for this calculation, the acronym for the index, and the units in which this is expressed.

Name	Variable (time aggregation)	Acronym	Units
WorldClim bioclimatic variables			
Annual mean temperature	tasmean (monthly)	BIO1	ºC
Annual means of maximum temperature*	tasmax (monthly)	BIO1max	ºC
Annual means of minimum temperature*	tasmin (monthly)	BIO1min	ºC
Seasonal mean temperature*	tasmean (monthly)	BIO1	ºC
Seasonal mean of maximum temperature*	tasmax (monthly)	BIO1max	ºC
Seasonal mean of minimum temperature*	tasmin (monthly)	BIO1min	ºC
Isothermality	tasmean (monthly)	BIO3	%
Temperature seasonality	pr (monthly)	BIO4	ºC
Maximum temperature of warmest month	tasmax (monthly)	BIO5	ºC
Minimum temperature of coldest month	tasmin (monthly)	BIO6	ºC
Annual temperature range	tasmax, tasmin (monthly)	BIO7	ºC
Mean temperature in wettest quarter	tasmean (monthly)	BIO8	ºC
Mean temperature in driest quarter	tasmean (monthly)	BIO9	ºC
Annual precipitation	pr (monthly)	BIO12	$kg\ m^{-2}$
Seasonal precipitation*	pr (monthly)	BIO12*	$kg\ m^{-2}$
Precipitation of wettest month	pr (monthly)	BIO13	$kg\ m^{-2}$
Precipitation seasonality	pr (monthly)	BIO15	%
Precipitation in the coldest quarter	pr (monthly)	BIO19	$kg\ m^{-2}$
ETCCDI extreme indices			
Daily temperature range	tasmax, tasmin (daily)	DTR (BIO2)	ºC
warmest day	tasmax (daily)	TXx	ºC
coldest night	tasmin (daily)	TNn	ºC
Growing season length	tasmean (daily)	GSL	days/year
Icing days	tasmax (daily)	ID	days/year
Frost days*	tasmin (daily)	TNltm2	days/year
wet days	pr (daily)	R1mm	days/year
Heavy precipitation days	pr (daily)	R10mm	days/year
Very heavy precipitation days	pr (daily)	R20mm	days/year
Simple daily Intensity	pr (daily)	SDII	$kg\ m^{-2}$
Wettest pentad	pr (daily)	Rx5day	$kg\ m^{-2}$
Maximum length of dry spell	pr (daily)	CDD	days/year
Precipitation-hour extreme indices			
Wet-hour frequency	pr (hourly)	$F_{wet-hour}$	%
Wet-hour intensity	pr (hourly)	$I_{wet-hour}$	$kg\ m^{-2}$
Maximum amount in the wettest month	pr (hourly)	PRWw	$kg\ m^{-2}$

3. Results

3.1. Temperature and precipitation distributions

Fig. 2 shows the probability density functions (PDFs) of tasmean (Fig. 2a) and pseudo-PDFs of pr (Fig. 2b), as well as the annual cycles of monthly values of both variables (Figs. 2c and 2d) for reference climate datasets and HighResClimNevada. WRF data from the parent domain (05-WRF) have also been included because they are closer in spatial resolution to the reference datasets and hence more comparable. To obtain the PDFs, pseudo-PDFs, and annual cycles, all grid points in the SN Natural Park were considered. PDFs were estimated using a 0.5 ºC bin, whereas pseudo-PDFs were obtained using an approach similar to that provided in Argüeso et al. (2012). That is, considering all grid points within the National and Natural Park borders, pseudo-PDFs for each dataset were obtained by grouping events of daily precipitation (pr > 0.1 mm) into 2 mm bins. The number of events multiplied by the mean intensity for each bin was then determined by dividing the total precipitation amounts (expressed in mm) for each bin by the number of grid points and days. Pseudo-PDFs were selected instead of the traditional PDFs in order to avoid masking light precipitation and, more importantly, heavy precipitation events.

In general, HighResClimNevada tasmean shows similar PDFs to other climate products (values ranging from -15 to 35 ºC) with certain bimodal features with two peaks of frequency (the highest peak around 5 ºC, while the lighter one is around 20 ºC). ROCIO_IBEB shows the greatest difference in the shape of the distribution, which exhibits a more diffuse bimodal character with its second mode shifted towards higher values. In terms of precipitation (Fig. 2b), differences between pseudo-PDFs are shown depending on the spatial resolution and the nature of the data. Events with pr around 10 mm/day seem to contribute to the highest amount of precipitation in HighResClimNevada. CHIRPS shows a similar shape in its pseudo-PDF but slightly shifted towards higher precipitation events. For the other climatic products, however, the highest amount of pr occurs for lighter events (5 mm/day or less), which is more pronounced in GPM IMERG and ERA5-Land. The latter suggests that the shape of the PDF is influenced, at least in part, by the spatial resolution of the data.

HighResClimNevada exhibits an annual cycle of monthly tasmean similar to 05-WRF and ROCIO_IBEB (Fig. 2c). However, underestimations of roughly 3 ºC are shown compared to ERA5-Land and slight overestimations when CERRA is employed as a reference. In any case, all climatic products reveal an annual cycle with the highest temperature in July and the lowest in January. Concerning the spatiotemporal distribution of temperature, the violin plot in Fig. 2c shows that HighResClimNevada, 05-WRF, and CERRA are more widespread, which could be related to the spatial resolution (the higher the spatial resolution, the greater the dispersion) and the nature of the data, as these three climatic products are derived from modeled data. It should be noted that in high mountain regions, the number of weather stations is limited, making temperature characterization more difficult for station-based products such as ROCIO_IBEB. Regarding precipitation, all climate products have a similar shape in their annual cycle (Fig. 2d), with the highest precipitation in December and the lowest during July. However, the amount of precipitation differs month by month. HighResClimNevada produces a high amount of pr (726 mm/year), second only to CHIRPS (792 mm/year) (inner figure in Fig. 2d), which is due to a higher amount of pr throughout the autumn and winter

months. However, compared to reanalysis-based data like CERRA-LAND or ERA5-Land, HighResClimNevada seems to
335 reveal a smaller pr amount throughout the summer.
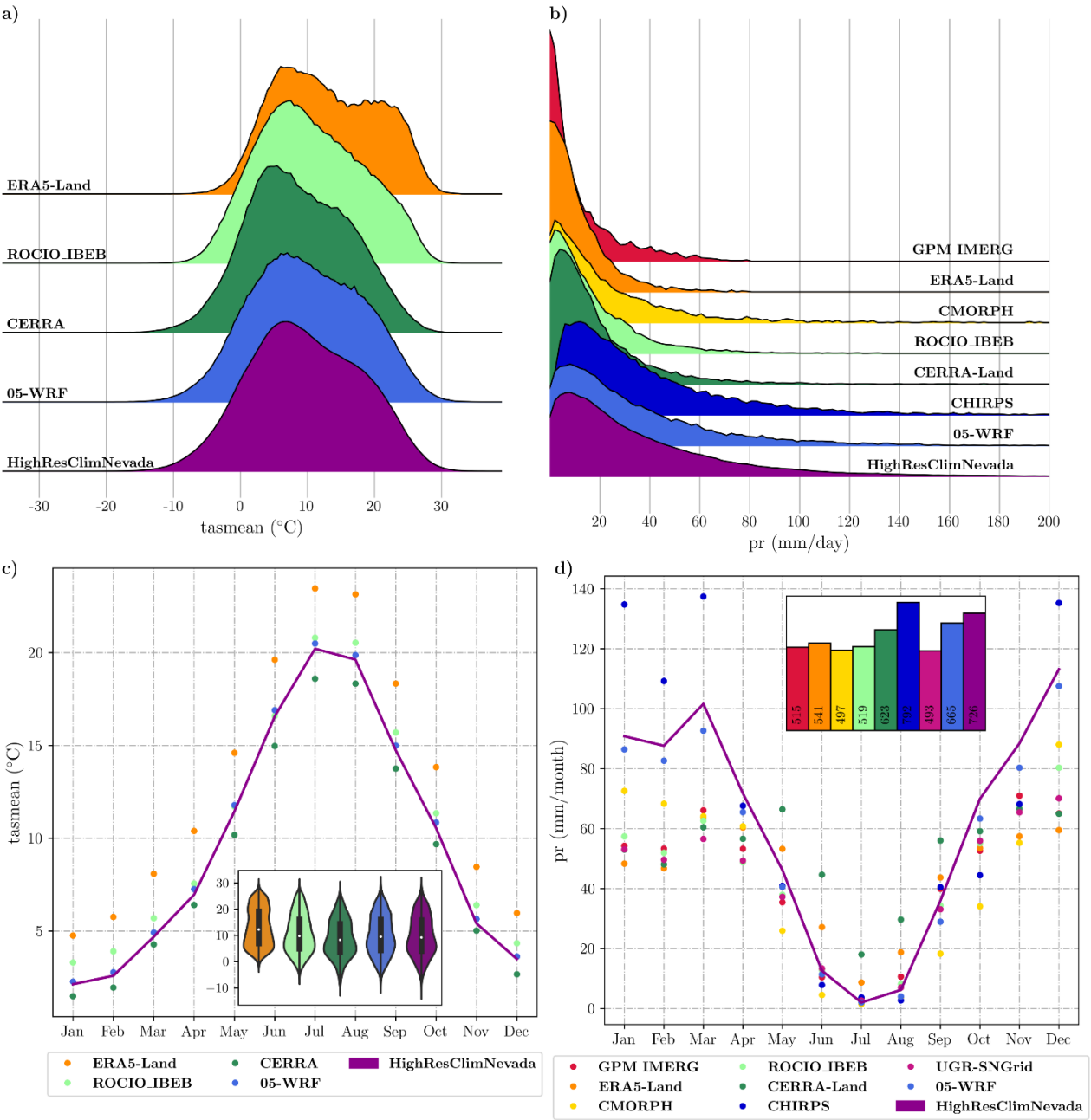
Figure 2: (a) Probability density functions (PDFs) of daily mean temperature (tasmean) and (b) pseudo-PDFs of the daily precipitation (pr) for all climatic products. Annual cycle of the monthly mean (c) temperature and (d) precipitation. The inner figure at c shows a violin plot with the monthly mean temperature values at each grid point and for each database. The inner figure at d
340 **shows a bar chart with the average annual precipitation amount (expressed in millimetres per year) in each database.**

3.2. Temperature and precipitation bioclimatic variables and extremes

Fig. 3 depicts the annual average of tasmax ($BIO1_{max}$), tasmean (BIO1), and tasmin ($BIO1_{min}$) for reference datasets (ERA5-Land, ROCIO_IBEB, and CERRA) and modeled data (05-WRF and HighResClimNevada). The dots in each panel represent the temperature recorded by SAIH stations. All climatic products are represented in their native spatial resolution to avoid problems caused by the interpolation method and the difference between spatial resolutions. Additionally, the temporal evolution of temperature in the Natural Park is depicted as warming stripes or standardized anomalies (i.e., annual temperature minus the annual mean in the common period, 2001-2020, divided by its standard deviation) under each map. Blue colors represent cooler than average years, while red colors suggest warmer than normal years. Blue and red intensities represent the magnitude of the anomaly. BIO1 characterizes the amount of energy captured by an ecosystem during a year, making its knowledge highly relevant for the conservation of high mountain ecosystems. In general, results show that temperature values ($BIO1_{max}$, BIO1, and $BIO1_{min}$) are very influenced by elevation, with the lowest values over the highest mountain peaks. All climatic products exhibit both similar spatial patterns and interannual variability, the latter as shown by warming stripes. These results, moreover, evidence the effect of spatial resolution. That is, datasets with coarser spatial resolution show more homogeneous temperature patterns, as they are not able to capture the elevation effects adequately. As a result, temperature in the Mulhacen and Veleta peaks in these datasets is usually higher (e.g., while ERA5-Land shows $BIO1_{min}$ values around 7 ºC in the highest altitudes, HighResClimNevada indicates values around -2 ºC). Moreover, HighResClimNevada produces comparable values to those from SAIH stations, as observed in 05-WRF, CERRA, and ROCIO_IBEB. However, ERA5-Land tends to overestimate both $BIO1_{max}$, BIO1, and $BIO1_{min}$. Comparable results can be found for seasonal values (Figs. S1-S4 in the supplementary figures).

HighResClimNevada, as other climatic products, accurately captures the main spatial patterns of annual precipitation in SN, showing an east-southwest gradient (Fig. 4). However, when we focus on high elevation areas, differences emerge that are determined by the spatial resolution and the nature of the data. Thus, in this region, downscaled fields (i.e., HighResClimNevada and 05-WRF), high-resolution satellite-derived products (CHIRPS), and high-resolution reanalysis (CERRA-Land) exhibit higher annual precipitation (greater than 1100 mm) than station-based data (ROCIO_IBEB and UGR-SNGrid), and others satellite-based and reanalysis data with lower resolution (GPM IMERG and ERA5-Land), where annual precipitation ranged from 550 to 700 mm approximately. These findings suggest the importance of spatial resolution in representing this variable, as datasets with resolutions of 5 km (or less) show a significant peak in annual cumulative precipitation at higher altitude. Lower-resolution datasets, on the other hand, exhibit more homogeneous precipitation patterns. This behavior is also shown in UGR-SNGrid and ROCIO_IBEB, where stations at high altitudes for precipitation calculation are very scarce. In comparison to the SAIH stations, HighResClimNevada shows higher BIO12, particularly at high altitude, where UGR-SNGrid produces closer values to these stations. It should be noted that the SAIH stations were one of the data sources in the development of UGR-SNGrid; therefore, similarities between the two are expected. It is also important to highlight the challenge of maintaining high mountain weather stations due to their limited accessibility, especially during storm

events when observed values are likely to be lower than those actually occurring. As a result, we know that, while these stations are reasonably good, their geographical position limits their quality. Grids based on these values are so likely to inherit this type of problem. HighResClimNevada presents a general agreement with other climatic products in the interannual variability of precipitation, as shown by the drying stripes. Similar conclusions can be drawn regarding the amount of precipitation that falls on average during winter (Fig. S5 in the supplementary material) and spring (Fig. S6). For summer (Fig. S7), all climatic products show precipitation values lower than 75 mm except for CERRA-Land and SAIH stations, which have precipitation values above 125, although in different locations. For autumn (Fig. S8), WRF outputs and CERRA-Land again show pr above 300 mm in the northwest, which is not replicated by other climatic products. However, for this season, the spatial pattern across the National Park appears to be more accurate than in other climatic products when compared to SAIH stations.
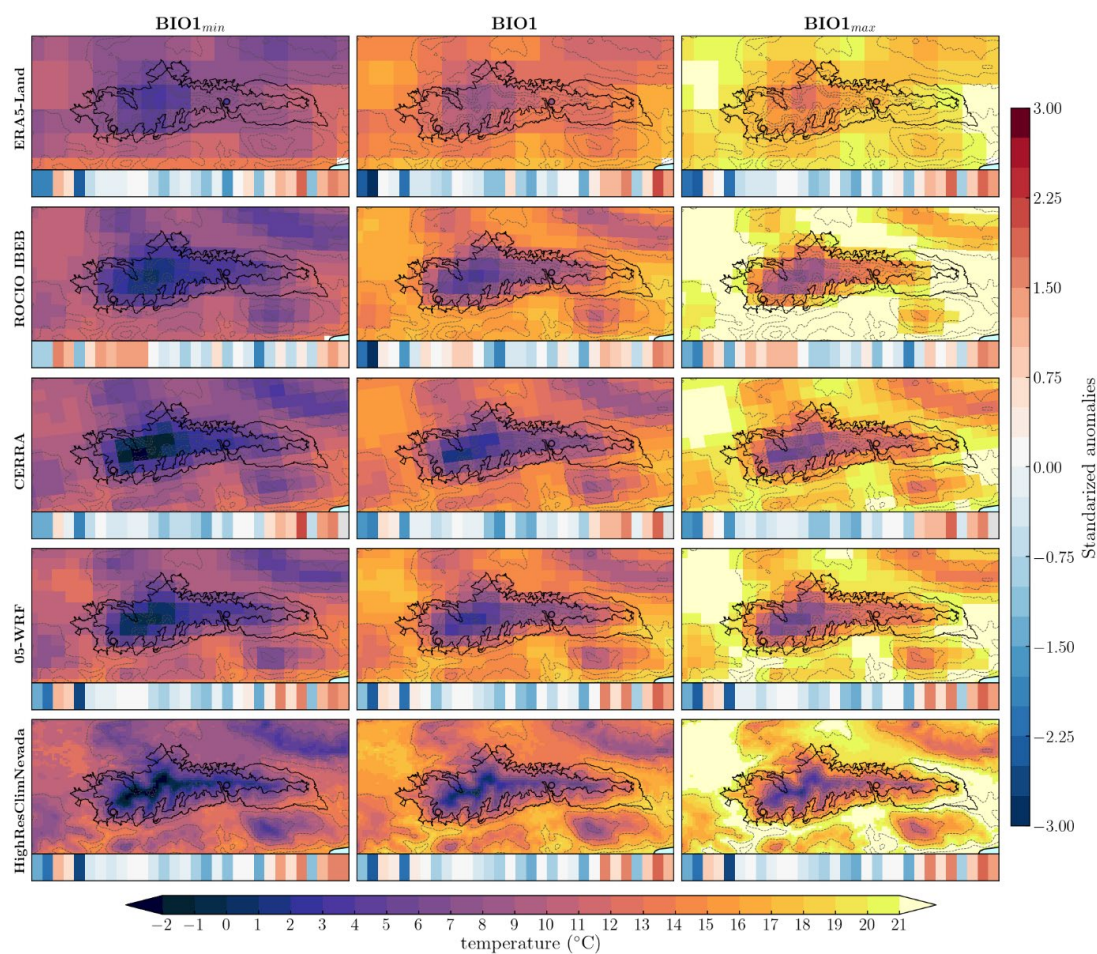
Figure 3: Annual average of the daily minimum, mean, and maximum temperatures (BIO1$_{min}$, BIO1, and BIO1$_{max}$) for each reference dataset (ERA5-Land, ROCIO_IBEB, and CERRA) as well as for downscaled data (05-WRF and HighResClimNevada). The dots in each panel represent the temperature recorded by SAIH stations, and the black solid lines display the National and Natural Park boundaries. Normalized anomalies for SN Natural Park over the period 2001-2020 for each database are shown below the corresponding spatial map in the form of warming stripes. In this representation, red colors indicate positive standardized anomalies, and blue colors correspond to negative values compared to the mean value for the whole period.

390
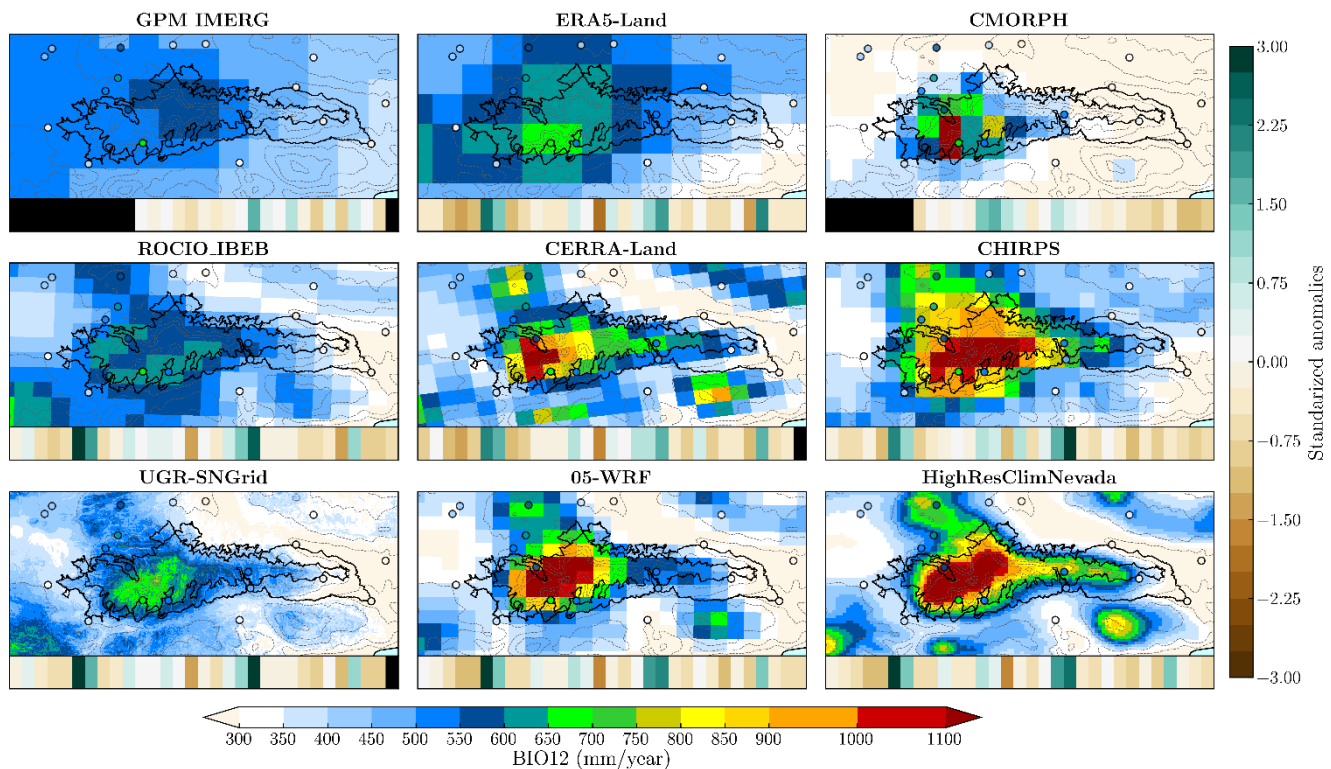
Figure 4: Average of the annual precipitation (BIO12, mm/year) for station-based data (ROCIO_IBEB and UGR-SNGrid), satellite image-based data (GPM IMERG, CMORPH, and CHIRPS), reanalysis data (ERA5-Land and CERRA-Land), and downscaled precipitation data (05-WRF and HighResClimNevada). The dots in each panel represent the precipitation recorded by SAIH stations and the black solid lines display the National and Natural Park boundaries. The annual standardized anomalies over the period
395 **2001-2020 for each database are shown below the corresponding spatial map in the form of drying stripes. In this representation, green colors indicate wet anomalies and brown colors the negative ones. Black colors indicate no data for that year.**

Fig. 5 depicts the long-term mean spatial patterns of temperature bioclimatic variables (Figs. from 5a to 5f) and ETCCDI extreme indices (Figs. 5g to 5l) for HighResClimNevada. In each panel, dots represent the corresponding values for SAIH

400   stations. In general, HighResClimNevada shows a comparable climate behavior to other products (Figs. S9 to S12) and stations, but with an apparent improvement due to the enhanced resolution. That is, HighResClimNevada characterizes orography-related effects that are not well captured by coarser climatic products like ERA5-Land (Fig. S9). In this regard, elevation influences most of the bioclimatic variables and extremes except for BIO4 and BIO7. Isothermality (BIO3, Fig. 5a) is a bioclimatic measure that compares variability within the day (BIO2 or DTR, Fig. 5g) to variability throughout the year

405   (BIO7, Fig. 5c). BIO3 is crucial for ecosystems, as many species might suffer damage in their population distribution as a result of daily and annual oscillations (O'Donnell and Ignizio, 2012). Values above 100% indicate that daily temperature variability is equal to the annual variability. According to HighResClimNevada, SN has low BIO3 (up to 35%), indicating that temperature fluctuations in this region during the day account for no more than 35% of the total variation across the year. The lowest BIO3 are depicted over the highest peaks, where they reach values less than 25%. In this region, DTR is also the lowest

410 in this region, with values falling below 6 °C. BIO7, however, reaches values between 23 °C and 30 °C, with the maximum located in the northeast of the Natural Park of SN. Like BIO7, temperature seasonality (BIO4) illustrates the temperature variability throughout the year. HighResClimNevada (Fig. 5b), with values between 6 °C and 7 °C, has the highest BIO4 values in the northeastern part of the Natural Park. For this variable, although the results of other climatic products are within the same range, their spatial patterns differ significantly. BIO5 (Fig. 5d), BIO8 (Fig. 5e), and BIO9 (Fig. 5f) are useful when we

415 are interested in analyzing if species distributions are affected by warm, wet, and dry temperatures, respectively (O'Donnell and Ignizio, 2012). Although HighResClimNevada is comparable to other climatic products in terms of these variables (see Figs. S9-S12d, S9-S12e, and S9-S1f), it appears to show lower values, especially when compared to ERA5-Land and ROCIO_IBEB, higher in the highest peaks. Similarly, HighResClimNevada has higher TNltm2 (Fig. 5l) and ID (Fig. 5k) than other climatic products, with values exceeding 160 and 105 days per year, respectively. TNltm2 and ID have critical

420 significance for ecosystems, as prolonged cold temperatures may cause considerable damage, affecting the survival of plant and animal species (Liu et al., 2018). GSL is a key variable in vegetable ecosystems because it influences essential functions including hydrology, nutrient cycling, productivity, and climate feedback (Barnard et al., 2018). In terms of this variable, HighResClimNevada shows values varying from 270 days/year in the outermost parts of the SN Natural Park to values below 90 days/year on the highest peaks (Fig. 5j), which is very similar to other climate products.

425 Fig. 6 depicts the interannual climate variability of bioclimatic variables and temperature extreme ETCCDI indices through the normalized anomalies in the area delimited by the SN Natural Park and estimated using the mean and standard deviation during the common period (2001-2020). For each index, the four databases, i.e., the three reference temperature datasets and HighResClimNevada, are plotted according to the order defined by the legend, with the color in each triangle representing the normalized anomaly for that year. Triangles colored in shades of red indicate that the index takes a value above normal, and

430 blue is the opposite pattern. In this figure, grey triangles indicate that there are no values in that dataset for that year. Overall, HighResClimNevada has a very similar temporal evolution to other climate products in terms of bioclimatic variables (from BIO3 to BIO9), suggesting that it is able to capture the SN temperature interannual variability. Thus, in general, anomalies in HighResClimNevada coincide in sign with those from other climatic products, but also in magnitude. That is all climatic products exhibited very high (low) BIO3 anomalies in 1997 (2012), with BIO7 lower (higher) than normal. Note that BIO7 is

435 the denominator for BIO3. This result indicates a small (high) dispersion in monthly temperature in that year when compared to the long-term climate, which is corroborated by BIO4. In the same way, BIO5 and BIO6 also agree in all products for 1997 (2012), showing that the maximum temperature of the warmest month was lower (higher) than normal, and the minimum temperature of the coldest month was higher (lower) than normal. Moreover, these years showed an unusually low (high) temperature in the driest quarter for that year, as indicated by BIO9. In the same way, temperature extremes are also similar in

440 all climatic products, suggesting also that HighResClimNevada captures the interannual variability of extreme temperature. Precipitation bioclimatic variables and extremes for HighResClimNevada are represented in Fig. 7. The dots in each panel reflect the values achieved by SAIH stations, while the black solid lines display the National and Natural Park boundaries. In general, the results suggest that orography influences the patterns of bioclimatic indices when the precipitation is implicated.

This is especially shown in the patterns of the precipitation of the wettest month (BIO13, Fig. 7a) and the precipitation of the coldest quarter (BIO19, Fig. 7c). Moreover, both variables show a very similar spatial pattern, with BIO13 values ranging from 90 to 350 mm and BIO19 values from 150 to 750 mm. Precipitation seasonality (BIO15, Fig. 7b), with values ranging from 95 to 120%, however, appears not to be influenced by orography, showing the lowest values in the north-northwest part of the SN National Park. Extreme ETCCDI indices are also influenced by orography (from Fig. 7d to Fig. 7i). That is, these indices show the highest extreme precipitation at high altitude in the western mountains and the lowest in the outermost Natural Park's regions. Thus, SN is characterized by R1mm (Fig. 7d), on average, between 35 and 80 rainy days per year, SDII values (Fig. 7g) ranging from 8 and 18 mm/day, and Rx5day (Fig. 7h) with values between 30 and 140 mm per 5 days. Heavy (R10mm, Fig. 7e) and very heavy (R20mm, Fig. 7f) precipitation days, on the other hand, exhibit similar regional patterns to R1mm, with maximum values exceeding 36 and 26 days per year, respectively. In terms of dry spells (CDD, Fig. 7i), HighResClimNevada indicates that the SN Natural Park is affected by 50 to 120 consecutive dry days. In terms of very extreme precipitation values (from Fig. 7j to Fig. 7l), which are based on hourly precipitation, HighResClimNevada shows that wet hours (hourly pr > 0.1 mm) account for 11% of the annual hours at the highest peaks, with values falling below 2% in the southeastern part of the SN National Park (Fig. 7j). The average intensity in wet hours appears to be around 1.6 mm/hour (Fig. 7k), with extreme hourly precipitation up to 25 mm/hour (Fig. 7l). For these latter indices, the orography has an unclear effect, with the highest values in the west and the south.

When the temporal evolution of precipitation values from HighResClimNevada is compared with other climatic products (Fig. 8), we can note more discrepancies than for temperature in the sign of the anomalies. Such discrepancies are greater when HighResClimNevada is compared to CMORPH, but the latter also disagrees with other climatic products. For example, in 2010, a year characterized by high precipitation records in the southern part of IP during the winter and spring, strong positive anomalies in BIO19 (i.e., precipitation of the coldest quarter) are depicted except for CMORPH, which indicates normal conditions for that year. Similarly, positive anomalies are observed for BIO13 (i.e., precipitation of the wettest month), but they are lighter than for BIO19. In terms of BIO15 (i.e., precipitation seasonality), however, there is not a clear consensus between datasets for that year. Very extreme precipitation indices indicate that HighResClimNevada performs well according to reference datasets providing hourly data (i.e., GPM IMERG, ERA5-Land, and CMORPH).

4.   Data and code availability

Codes, supplementary figure and HighResClimNevada data are available in García-Valdecasas Ojeda et al. (2024) (https://doi.org/10.5281/zenodo.14883471). In this link, daily values of temperature (mean, maximum, and minimum), precipitation, near-surface relative humidity, surface pressure, surface net radiation, and wind speed for the region of Sierra Nevada at 1 km spatial resolution can be found. Additionally, hourly precipitation and temperature datasets are provided as a part of this database as well as bioclimatic variables and extremes. For the evaluation of our HighResClimNevada, different reference data were used, all freely available. AEMET 5km gridded datasets (ROCIO_IBEB version 2) are online available at

Figure 5: Spatial patterns of temperature bioclimatic variables and extreme ETCCDI indices in HighResClimNevada. (a) Isothermality (BIO3,%), (b) temperature seasonality (BIO4, ºC), (c) annual temperature range (BIO7, ºC), (d) maximum temperature of warmest month (BIO5, ºC), (e) mean temperature of wettest quarter (BIO8, ºC), (f) mean temperature of driest quarter (BIO9, ºC), (g) daily temperature range (DTR, ºC), (h) maximum warmest day (TXx, ºC), (i) minimum coldest night (TNn, ºC), (j) growing season length (GSL, days/year), (k) icing days (ID, days/year), and (l) frost days (TNltm2, days/year). The dots in each panel reflect the values achieved by SAIH stations, while the black solid lines display the National and Natural Park boundaries.
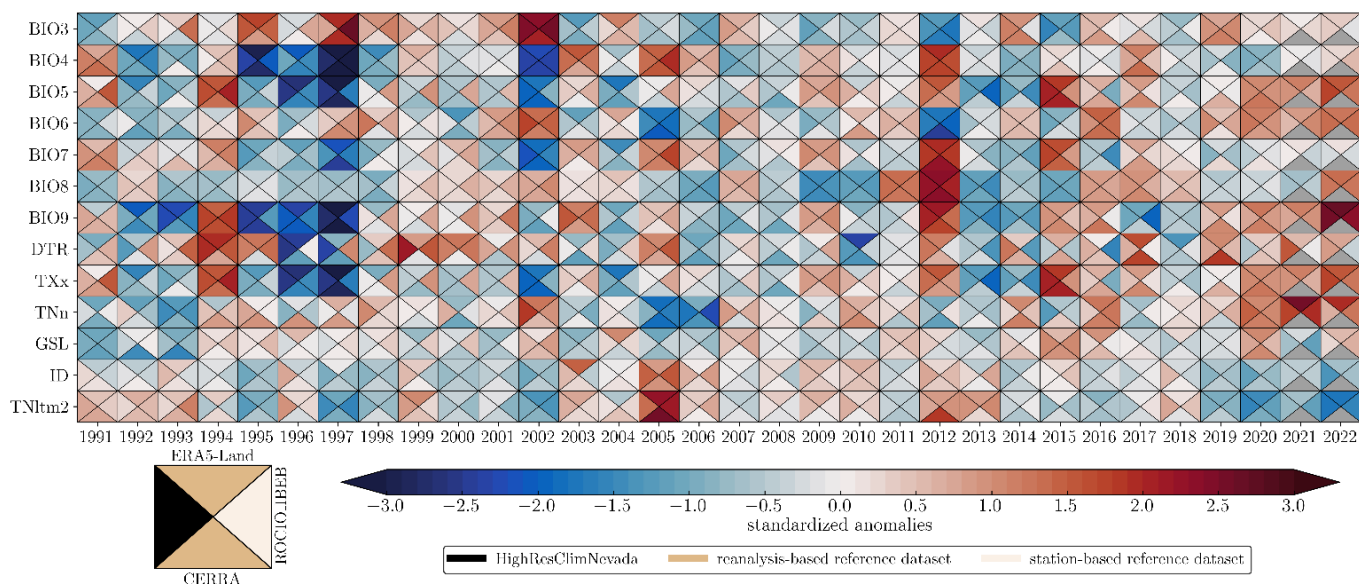
495 **Figure 6: Normalized temperature anomalies for bioclimatic variables and ETCCDI extreme indices. Anomalies are calculated using the mean and standard deviation in a common period (1991-2022) of each database and spatially averaged across the SN Natural Park. Grey triangles indicate that there is no value for that year in the specified database. The legend depicts the sequence of data in each square (in black, HighResClimNevada), with the nature of each database marked by color.**

5.   Discussion and conclusions

500   We present HighResClimNevada, a climatological 1-km dataset derived from regional climate modeling. To do that, the Weather Research and Forecasting model v4.3.3 with a configuration especially designed for Sierra Nevada has been used. SN is a region of special interest due to its high ecological value. Therefore, HighResClimNevada has been developed with the purpose of filling the gap of lack of long-term climate information regular in space and time using climate modeling. This database has been generated based only on climate model outputs and therefore it does not consider information from

505   observations of ground-based stations or satellites via assimilation in order to avoid new sources of uncertainties. Note, observations in this region are usually short and contain errors due to instrumental inaccuracies or poorly calibrated equipment since SN is an area of difficult access. Furthermore, satellite information frequently has substantial uncertainties and short records; hence, assimilation may contribute additional uncertainty into climate data. HighResClimNevada provides hourly and daily primary climate variables structured in netCDF files with variables stored in a 1-km grid from January 1991 to December

510   2022.

Additionally, and due to the special relevance of this region to study the impacts of climate change, bioclimatic variables, extreme ETCCDI climate indices, as well as hour-precipitation extreme indices derived from hourly precipitation were postprocessed and are also part of this climatic product. HighResClimNevada was compared with reference datasets in order to evaluate its climate performance. These comparisons showed that HighResClimNevada is a valuable tool for assessing

trends in temperature variables, both in terms of extreme and mean values, as its performance is similar to that of other products. However, due to its higher resolution, it shows a level of spatial detail that is not available in the other products, which is physically consistent (due to the nature of the product itself) and necessary for ecological analysis. In terms of precipitation, more discrepancies are shown, although it is important to note the difficulty in obtaining data in this complex region. In fact, it is well known that datasets based on observations often have problems in high mountain regions due to the challenge of maintaining station networks with an adequate density of stations. Moreover, satellite products like GPM IMERG or CMORPH also show problems characterizing the precipitation amount fallen over mountains, leading to underestimations (Derin and Yilmaz, 2014; Kazamias et al., 2022; Navarro et al., 2020; Tapiador et al., 2020). However, HighResClimNevada shows a similar behavior in many extreme values to reanalysis products such as CERRA-Land and CHIRPS. The HighResClimNevada dataset presented here serves as a scientific basis for assessing the impacts of climate change over SN on many sectors, such as on ecological and hydrological systems.
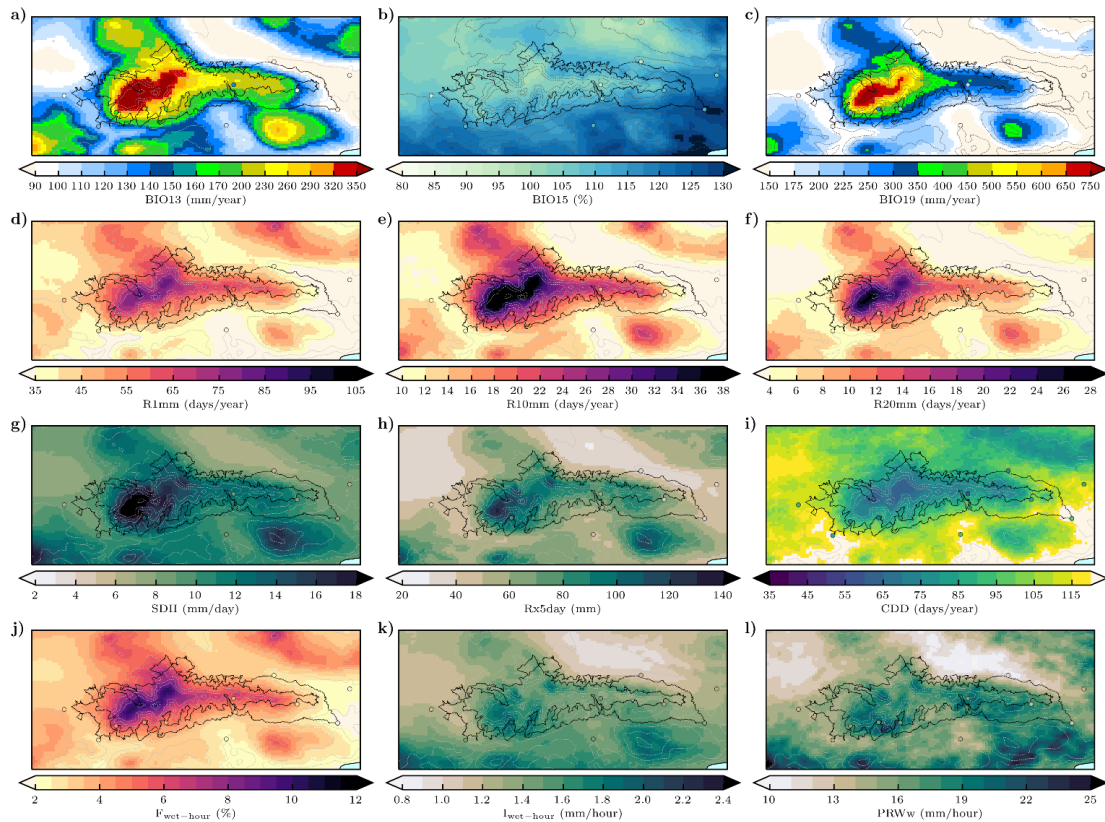
Figure 7: Spatial patterns of bioclimatic variables and extreme ETCCDI indices of precipitation in HighResClimNevada. (a) precipitation of wettest month (BIO13, mm/month), (b) precipitation seasonality (BIO15, mm/month), (c) precipitation in the coldest quarter (BIO19, mm/month), (d) wet days (R1mm, days/year), (e) heavy precipitation days (R10mm, days/year), (f) very heavy precipitation days (R20mm, days/year), (g) simple daily intensity index (SDII, mm/year), (h) maximum 5-day precipitation (Rx5day, mm), (i) consecutive dry days (CDD, days/year), (j) wet-hour frequency (F$_{wet-day}$, %), (k) wet-hour intensity (I$_{wet-day}$, mm/hour), and (l) maximum amount in the wettest month (PRWw, mm/hour). The dots in each panel reflect the values achieved by SAIH stations, while the black solid lines display the National and Natural Park boundaries.
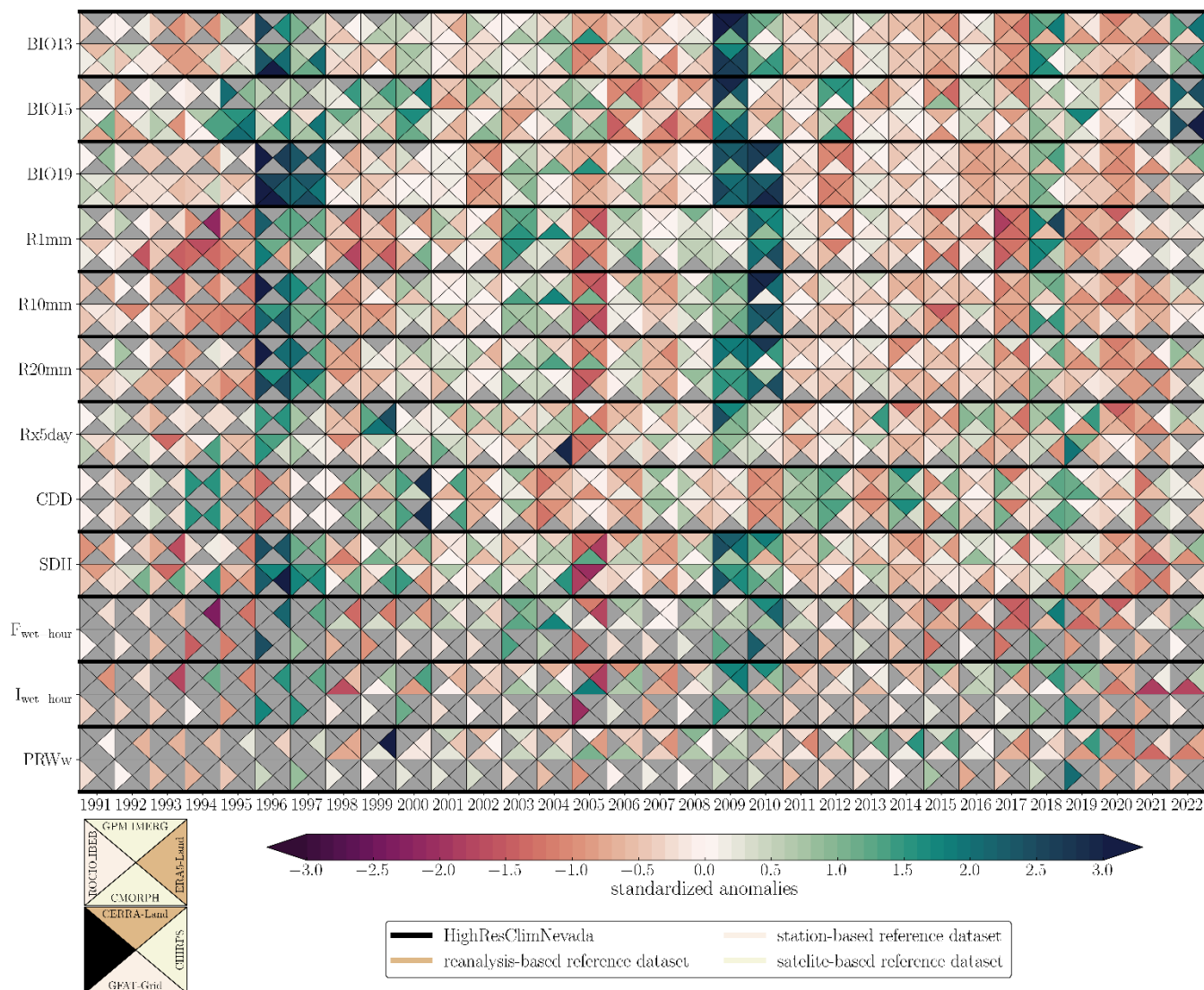
Figure 8: Normalized precipitation anomalies for bioclimatic variables, ETCCDI extreme indices, and precipitation-hour extreme indices. Anomalies are calculated using the mean and standard deviation in a common period (1991-2022) of each database and spatially averaged across the SN Natural Park. Green colours indicate wet anomalies while red colours show drier than normal values. Grey triangles indicate that there is no value for that year in the specified database. The legend depicts the sequence of the data in each square (in black, HighResClimNevada), with the nature of each database marked by colours.

Acknowledgement: This research was financially supported by the project "Plan Complementario de I+D+i en el área de Biodiversidad (PCBIO)" funded by the European Union within the framework of the Recovery, Transformation and Resilience Plan - NextGenerationEU and by the Regional Government of Andalucia, Grant BIOD2022_002, funded by Consejería de Universidad, Investigación e Innovación and Gobierno de España and Unión Europea – NextGenerationEU, from Biorefuges (TED2021-130888B-I00) funded by MCIN/AEI/10.13039/501100011033 and by the European Union, and by the project

PID2021-126401OB-I00, funded by MICIU/AEI/10.13039/501100011033 and by FEDER, UE; The authors thank the editor and the anonymous referees for their insightful comments that have helped to improve this work.

Competing interests: The contact author has declared that none of the authors has any competing interests.

550 ## 6. References

Alzate Velásquez, D. F., Araujo Carrillo, G. A., Rojas Barbosa, E. O., Gomez Latorre, D. A., and Martínez Maldonado, F. E.: Interpolacion Regnie para lluvia y temperatura en las regiones andina, caribe y pacífica de Colombia, Colomb. for., 21, 102, https://doi.org/10.14483/2256201X.11601, 2017.

Argüeso, D., Hidalgo-Muñoz, J. M., Gámiz-Fortis, S. R., Esteban-Parra, M. J., and Castro-Díez, Y.: Evaluation of WRF Mean

555 and Extreme Precipitation over Spain: Present Climate (1970–99), Journal of Climate, 25, 4883–4897, https://doi.org/10.1175/JCLI-D-11-00276.1, 2012.

Bae, S. Y., Hong, S.-Y., and Tao, W.-K.: Development of a Single-Moment Cloud Microphysics Scheme with Prognostic Hail for the Weather Research and Forecasting (WRF) Model, Asia-Pacific J Atmos Sci, 55, 233–245, https://doi.org/10.1007/s13143-018-0066-3, 2019.

560 Barnard, D. M., Knowles, J. F., Barnard, H. R., Goulden, M. L., Hu, J., Litvak, M. E., and Molotch, N. P.: Reevaluating growing season length controls on net ecosystem production in evergreen conifer forests, Sci Rep, 8, 17973, https://doi.org/10.1038/s41598-018-36065-0, 2018.

Begert, M. and Frei, C.: Long-term area-mean temperature series for Switzerland—Combining homogenized station data and high resolution grid data, Intl Journal of Climatology, 38, 2792–2807, https://doi.org/10.1002/joc.5460, 2018.

565 Beniston, M.: Climatic Change in Mountain Regions: A Review of Possible Impacts, Climatic Change, 59, 5–31, https://doi.org/10.1023/A:1024458411589, 2003.

Beniston, M., Farinotti, D., Stoffel, M., Andreassen, L. M., Coppola, E., Eckert, N., Fantini, A., Giacona, F., Hauck, C., Huss, M., Huwald, H., Lehning, M., López-Moreno, J.-I., Magnusson, J., Marty, C., Morán-Tejéda, E., Morin, S., Naaim, M., Provenzale, A., Rabatel, A., Six, D., Stötter, J., Strasser, U., Terzago, S., and Vincent, C.: The European mountain cryosphere:

570 a review of its current state, trends, and future challenges, The Cryosphere, 12, 759–794, https://doi.org/10.5194/tc-12-759-2018, 2018.

Blanca, G., Cueto, M., Martínez-Lirola, M. J., and Molero-Mesa, J.: Threatened vascular flora of Sierra Nevada (Southern Spain), Biological Conservation, 85, 269–285, https://doi.org/10.1016/S0006-3207(97)00169-9, 1998.

Collins, W., Rasch, P., Boville, B., McCaa, J., Williamson, D., Kiehl, J., Briegleb, B., Bitz, C., Lin, S.-J., Zhang, M., and Dai,

575 Y.: Description of the NCAR Community Atmosphere Model (CAM 3.0), UCAR/NCAR, https://doi.org/10.5065/D63N21CH, 2004.

Coppola, E., Sobolowski, S., Pichelli, E., Raffaele, F., Ahrens, B., Anders, I., Ban, N., Bastin, S., Belda, M., Belusic, D., Caldas-Alvarez, A., Cardoso, R. M., Davolio, S., Dobler, A., Fernandez, J., Fita, L., Fumiere, Q., Giorgi, F., Goergen, K., Güttler, I., Halenka, T., Heinzeller, D., Hodnebrog, Ø., Jacob, D., Kartsios, S., Katragkou, E., Kendon, E., Khodayar, S., Kunstmann, H., Knist, S., Lavín-Gullón, A., Lind, P., Lorenz, T., Maraun, D., Marelle, L., Van Meijgaard, E., Milovac, J., Myhre, G., Panitz, H.-J., Piazza, M., Raffa, M., Raub, T., Rockel, B., Schär, C., Sieck, K., Soares, P. M. M., Somot, S., Srnec, L., Stocchi, P., Tölle, M. H., Truhetz, H., Vautard, R., De Vries, H., and Warrach-Sagi, K.: A first-of-its-kind multi-model convection permitting ensemble for investigating convective phenomena over Europe and the Mediterranean, Clim Dyn, 55, 3–34, https://doi.org/10.1007/s00382-018-4521-8, 2020.

Denis, B., Laprise, R., and Caya, D.: Sensitivity of a regional climate model to the resolution of the lateral boundary conditions, Climate Dynamics, 20, 107–126, https://doi.org/10.1007/s00382-002-0264-6, 2003.

Derin, Y. and Yilmaz, K. K.: Evaluation of Multiple Satellite-Based Precipitation Products over Complex Topography, Journal of Hydrometeorology, 15, 1498–1516, https://doi.org/10.1175/JHM-D-13-0191.1, 2014.

Esteban-Parra, M. J., García-Valdecasas Ojeda, M., Peinó-Calero, E., Romero-Jiménez, E., Yeste, P., Rosa-Cánovas, J. J., Rodríguez-Brito, A., Gámiz-Fortis, S. R., and Castro-Díez, Y.: Climate Variability and Trends, in: The Landscape of the Sierra Nevada, edited by: Zamora, R. and Oliva, M., Springer International Publishing, Cham, 129–148, https://doi.org/10.1007/978-3-030-94219-9_9, 2022.

Fick, S. E. and Hijmans, R. J.: WorldClim 2: new 1-km spatial resolution climate surfaces for global land areas, Intl Journal of Climatology, 37, 4302–4315, https://doi.org/10.1002/joc.5086, 2017.

Funk, C., Peterson, P., Landsfeld, M., Pedreros, D., Verdin, J., Shukla, S., Husak, G., Rowland, J., Harrison, L., Hoell, A., and Michaelsen, J.: The climate hazards infrared precipitation with stations—a new environmental record for monitoring extremes, Sci Data, 2, 150066, https://doi.org/10.1038/sdata.2015.66, 2015.

Garcia-Valdecasas Ojeda, M., Solano Farías, F., Donaire Montaño, D., Romero-Jiménez, E., Rosa-Cánovas, J. J., Gámiz-Fortis, S. R., Castro-Díez, Y., and Esteban-Parra, M. J.: HighResClimNevada: a high-resolution climatological dataset for a high-altitude region in Southern Spain (Sierra Nevada), https://doi.org/10.5281/ZENODO.14883471, 2025.

Gobiet, A., Kotlarski, S., Beniston, M., Heinrich, G., Rajczak, J., and Stoffel, M.: 21st century climate change in the European Alps—A review, Science of The Total Environment, 493, 1138–1151, https://doi.org/10.1016/j.scitotenv.2013.07.050, 2014.

González-Rojí, S. J., Messmer, M., Raible, C. C., and Stocker, T. F.: Sensitivity of precipitation in the highlands and lowlands of Peru to physics parameterization options in WRFV3.8.1, Geosci. Model Dev., 15, 2859–2879, https://doi.org/10.5194/gmd-15-2859-2022, 2022.

Grell, G. A. and Freitas, S. R.: A scale and aerosol aware stochastic convective parameterization for weather and air quality modeling, Atmos. Chem. Phys., 14, 5233–5250, https://doi.org/10.5194/acp-14-5233-2014, 2014.

Halladay, K., Berthou, S., and Kendon, E.: Improving land surface feedbacks to the atmosphere in convection-permitting climate simulations for Europe, Clim Dyn, https://doi.org/10.1007/s00382-024-07192-4, 2024.

Hartmann, D. L., Wallace, J. M., Limpasuvan, V., Thompson, D. W. J., and Holton, J. R.: Can ozone depletion and global warming interact to produce rapid climate change?, Proceedings of the National Academy of Sciences, 97, 1412–1417, https://doi.org/10.1073/pnas.97.4.1412, 2000.

Hersbach, H., Bell, B., Berrisford, P., Hirahara, S., Horányi, A., Muñoz-Sabater, J., Nicolas, J., Peubey, C., Radu, R., Schepers, D., Simmons, A., Soci, C., Abdalla, S., Abellan, X., Balsamo, G., Bechtold, P., Biavati, G., Bidlot, J., Bonavita, M., De Chiara, G., Dahlgren, P., Dee, D., Diamantakis, M., Dragani, R., Flemming, J., Forbes, R., Fuentes, M., Geer, A., Haimberger, L., Healy, S., Hogan, R. J., Hólm, E., Janisková, M., Keeley, S., Laloyaux, P., Lopez, P., Lupu, C., Radnoti, G., De Rosnay, P., Rozum, I., Vamborg, F., Villaume, S., and Thépaut, J.: The ERA5 global reanalysis, Quart J Royal Meteoro Soc, 146, 1999–2049, https://doi.org/10.1002/qj.3803, 2020.

Hijmans, R. J., Cameron, S. E., Parra, J. L., Jones, P. G., and Jarvis, A.: Very high resolution interpolated climate surfaces for global land areas, Int. J. Climatol., 25, 1965–1978, https://doi.org/10.1002/joc.1276, 2005.

Huffman, G. J., Stocker, E. F., Bolvin, D. T., Nelkin, E. J., and Jackson, T.: GPM IMERG Final Precipitation L3 Half Hourly 0.1 degree x 0.1 degree V06, https://doi.org/10.5067/GPM/IMERG/3B-HH/06, 2019.

Huffman, G. J., Bolvin, D. T., Braithwaite, D., Hsu, K.-L., Joyce, R. J., Kidd, C., Nelkin, E. J., Sorooshian, S., Stocker, E. F., Tan, J., Wolff, D. B., and Xie, P.: Integrated Multi-satellite Retrievals for the Global Precipitation Measurement (GPM) Mission (IMERG), in: Satellite Precipitation Measurement, vol. 67, edited by: Levizzani, V., Kidd, C., Kirschbaum, D. B., Kummerow, C. D., Nakamura, K., and Turk, F. J., Springer International Publishing, Cham, 343–353, https://doi.org/10.1007/978-3-030-24568-9_19, 2020.

Jerez, S., López-Romero, J. M., Turco, M., Lorente-Plazas, R., Gómez-Navarro, J. J., Jiménez-Guerrero, P., and Montávez, J. P.: On the Spin-Up Period in WRF Simulations Over Europe: Trade-Offs Between Length and Seasonality, J Adv Model Earth Syst, 12, e2019MS001945, https://doi.org/10.1029/2019MS001945, 2020.

Jiménez, P. A., Dudhia, J., González-Rouco, J. F., Navarro, J., Montávez, J. P., and García-Bustamante, E.: A Revised Scheme for the WRF Surface Layer Formulation, Monthly Weather Review, 140, 898–918, https://doi.org/10.1175/MWR-D-11-00056.1, 2012.

Joyce, R. J., Janowiak, J. E., Arkin, P. A., and Xie, P.: CMORPH: A Method that Produces Global Precipitation Estimates from Passive Microwave and Infrared Data at High Spatial and Temporal Resolution, J. Hydrometeor, 5, 487–503, https://doi.org/10.1175/1525-7541(2004)005<0487:CAMTPG>2.0.CO;2, 2004.

Karger, D. N., Conrad, O., Böhner, J., Kawohl, T., Kreft, H., Soria-Auza, R. W., Zimmermann, N. E., Linder, H. P., and Kessler, M.: Climatologies at high resolution for the earth's land surface areas, Sci Data, 4, 170122, https://doi.org/10.1038/sdata.2017.122, 2017.

Kazamias, A.-P., Sapountzis, M., and Lagouvardos, K.: Evaluation of GPM-IMERG rainfall estimates at multiple temporal and spatial scales over Greece, Atmospheric Research, 269, 106014, https://doi.org/10.1016/j.atmosres.2021.106014, 2022.

Khodayar, S., Sehlinger, A., Feldmann, H., and Kottmeier, Ch.: Sensitivity of soil moisture initialization for decadal predictions under different regional climatic conditions in Europe, Intl Journal of Climatology, 35, 1899–1915, https://doi.org/10.1002/joc.4096, 2015.

645 La Sorte, F. A. and Jetz, W.: Projected range contractions of montane biodiversity under global warming, Proc. R. Soc. B., 277, 3401–3410, https://doi.org/10.1098/rspb.2010.0612, 2010.

Liu, Q., Piao, S., Janssens, I. A., Fu, Y., Peng, S., Lian, X., Ciais, P., Myneni, R. B., Peñuelas, J., and Wang, T.: Extension of the growing season increases vegetation exposure to frost, Nat Commun, 9, 426, https://doi.org/10.1038/s41467-017-02690-y, 2018.

650 Lucas-Picher, P., Brisson, E., Caillaud, C., Alias, A., Nabat, P., Lemonsu, A., Poncet, N., Cortés Hernandez, V. E., Michau, Y., Doury, A., Monteiro, D., and Somot, S.: Evaluation of the convection-permitting regional climate model CNRM-AROME41t1 over Northwestern Europe, Clim Dyn, 62, 4587–4615, https://doi.org/10.1007/s00382-022-06637-y, 2024.

Matte, D., Laprise, R., and Thériault, J. M.: Comparison between high-resolution climate simulations using single- and double-nesting approaches within the Big-Brother experimental protocol, Clim Dyn, 47, 3613–3626, https://doi.org/10.1007/s00382-655 016-3031-9, 2016.

Messmer, M., González-Rojí, S. J., Raible, C. C., and Stocker, T. F.: Sensitivity of precipitation and temperature over the Mount Kenya area to physics parameterization options in a high-resolution model simulation performed with WRFV3.8.1, Geosci. Model Dev., 14, 2691–2711, https://doi.org/10.5194/gmd-14-2691-2021, 2021.

Muñoz-Sabater, J., Dutra, E., Agustí-Panareda, A., Albergel, C., Arduini, G., Balsamo, G., Boussetta, S., Choulga, M., 660 Harrigan, S., Hersbach, H., Martens, B., Miralles, D. G., Piles, M., Rodríguez-Fernández, N. J., Zsoter, E., Buontempo, C., and Thépaut, J.-N.: ERA5-Land: a state-of-the-art global reanalysis dataset for land applications, Earth Syst. Sci. Data, 13, 4349–4383, https://doi.org/10.5194/essd-13-4349-2021, 2021.

Navarro, A., García-Ortega, E., Merino, A., Sánchez, J. L., and Tapiador, F. J.: Orographic biases in IMERG precipitation estimates in the Ebro River basin (Spain): The effects of rain gauge density and altitude, Atmospheric Research, 244, 105068, 665 https://doi.org/10.1016/j.atmosres.2020.105068, 2020.

Nigrelli, G. and Chiarle, M.: 1991–2020 climate normal in the European Alps: focus on high-elevation environments, J. Mt. Sci., 20, 2149–2163, https://doi.org/10.1007/s11629-023-7951-7, 2023.

Noce, S., Caporaso, L., and Santini, M.: A new global dataset of bioclimatic indicators, Sci Data, 7, 398, https://doi.org/10.1038/s41597-020-00726-5, 2020.

670 O'Donnell, M. S. and Ignizio, D. A.: Bioclimatic predictors for supporting ecological applications in the conterminous United States, 2012.

Oliva, M., Fernández-Fernández, J. M., and Martín-Díaz, J.: The Geographic Uniqueness of the Sierra Nevada in the Context of the Mid-Latitude Mountains, in: The Landscape of the Sierra Nevada, edited by: Zamora, R. and Oliva, M., Springer International Publishing, Cham, 3–9, https://doi.org/10.1007/978-3-030-94219-9_1, 2022.

675 Parmesan, C.: Ecological and Evolutionary Responses to Recent Climate Change, Annu. Rev. Ecol. Evol. Syst., 37, 637–669, https://doi.org/10.1146/annurev.ecolsys.37.091305.110100, 2006.

Pepin, N., Deng, H., Zhang, H., Zhang, F., Kang, S., and Yao, T.: An Examination of Temperature Trends at High Elevations Across the Tibetan Plateau: The Use of MODIS LST to Understand Patterns of Elevation-Dependent Warming, JGR Atmospheres, 124, 5738–5756, https://doi.org/10.1029/2018JD029798, 2019.

680 Pepin, N. C., Arnone, E., Gobiet, A., Haslinger, K., Kotlarski, S., Notarnicola, C., Palazzi, E., Seibert, P., Serafin, S., Schöner, W., Terzago, S., Thornton, J. M., Vuille, M., and Adler, C.: Climate Changes and Their Elevational Patterns in the Mountains of the World, Reviews of Geophysics, 60, e2020RG000730, https://doi.org/10.1029/2020RG000730, 2022.

Peral García, C., Navascués Fernández-Victorio, B., and Ramos Calzado, P.: Serie de precipitación diaria en rejilla con fines climáticos, Agencia Estatal de Meteorología, https://doi.org/10.31978/014-17-009-5, 2017.

685 Pleim, J. E.: A Combined Local and Nonlocal Closure Model for the Atmospheric Boundary Layer. Part I: Model Description and Testing, Journal of Applied Meteorology and Climatology, 46, 1383–1395, https://doi.org/10.1175/JAM2539.1, 2007.

Polo, M. J., Herrero, J., Pimentel, R., and Pérez-Palazón, M. J.: The Guadalfeo Monitoring Network (Sierra Nevada, Spain): 14 years of measurements to understand the complexity of snow dynamics in semiarid regions, Earth Syst. Sci. Data, 11, 393–407, https://doi.org/10.5194/essd-11-393-2019, 2019.

690 Polo, M. J., Pimentel, R., Gascoin, S., and Notarnicola, C.: Mountain hydrology in the Mediterranean region, in: Water Resources in the Mediterranean Region, Elsevier, 51–75, https://doi.org/10.1016/B978-0-12-818086-0.00003-0, 2020.

Prein, A. F. and Gobiet, A.: Impacts of uncertainties in European gridded precipitation observations on regional climate analysis, Int. J. Climatol., 37, 305–327, https://doi.org/10.1002/joc.4706, 2017.

Prein, A. F., Langhans, W., Fosser, G., Ferrone, A., Ban, N., Goergen, K., Keller, M., Tölle, M., Gutjahr, O., Feser, F., Brisson, 695 E., Kollet, S., Schmidli, J., Van Lipzig, N. P. M., and Leung, R.: A review on regional convection-permitting climate modeling: Demonstrations, prospects, and challenges, Reviews of Geophysics, 53, 323–361, https://doi.org/10.1002/2014RG000475, 2015.

Prein, A. F., Rasmussen, R., and Stephens, G.: Challenges and Advances in Convection-Permitting Climate Modeling, Bulletin of the American Meteorological Society, 98, 1027–1030, https://doi.org/10.1175/BAMS-D-16-0263.1, 2017.

700 Prein, A. F., Rasmussen, R., Castro, C. L., Dai, A., and Minder, J.: Special issue: Advances in convection-permitting climate modeling, Clim Dyn, 55, 1–2, https://doi.org/10.1007/s00382-020-05240-3, 2020.

Rangwala, I. and Miller, J. R.: Climate change in mountains: a review of elevation-dependent warming and its possible causes, Climatic Change, 114, 527–547, https://doi.org/10.1007/s10584-012-0419-3, 2012.

Rauthe, M., Steiner, H., Riediger, U., Mazurkiewicz, A., and Gratzki, A.: A Central European precipitation climatology Part 705 I: Generation and validation of a high-resolution gridded daily data set (HYRAS), metz, 22, 235–256, https://doi.org/10.1127/0941-2948/2013/0436, 2013.

Romero-Jiménez, E., Cepeda-Ventura, L., García-Valdecasas Ojeda, M., Rosa-Cánovas, J. J., Donaire-Montaño, D., Solano-Farías, F., Toro Ortiz, Y., Gámiz-Fortis, S. R., Castro-Díez, Y., and Esteban-Parra, M. J.: Creating a gridded climate database in Sierra Nevada, in the southern Iberian Peninsula, , https://doi.org/10.5194/ems2023-463, 2023.

710 Romero-Jiménez, E., Cepeda-Ventura, L., García-Valdecasas Ojeda, M., Rosa-Cánovas, J. J., Castro-Díez, Y., Gámiz-Fortis, S. R., and Esteban-Parra, M. J.: UGR-SNGrid: Datos de Precipitación Mensual para Sierra Nevada, https://doi.org/10.5281/ZENODO.13885000, 2024.

Sangelantoni, L., Sobolowski, S., Lorenz, T., Hodnebrog, Ø., Cardoso, R. M. C., Soares, P., Ferretti, R., Lavín-Gullón, A., Fernandez, J., Goergen, K., Milovac, J., Katragkou, E., Kartsios, S., Coppola, E., Pichelli, E., Adinolfi, M., Mercogliano, P.,
715 Berthou, S., De Vries, H., Dobler, A., Belušić, D., Feldmann, H., Tölle, M., and Bastin, S.: Investigating the Representation of Heatwaves from an Ensemble of Km-scale Regional Climate Simulations within CORDEX-FPS Convection, https://doi.org/10.21203/rs.3.rs-1395524/v1, 2 March 2022.

Schimanke, S., Ridal, M., Le Moigne, P., Berggren, L., Undén, P., Randriamampianina, R., Andrea, U., Bazile, E., Bertelsen, A., Brousseau, P., Dahlgren, P., Edvinsson, L., El Said, A., Glinton, M., Hopsch, S., Isaksson, L., Mladek, R., Olsson, E.,
720 Verrelle, A., and Wang, Z. Q.: CERRA sub-daily regional reanalysis data for Europe on single levels from 1984 to present, https://doi.org/10.24381/CDS.622A565A, 2021.

Sigro, J., Cisneros, M., Perez-Luque, A. J., Perez-Martinez, C., and Vegas-Vilarrubia, T.: Trends in temperature and precipitation at high and low elevations in the main mountain ranges of the Iberian Peninsula (1894–2020): The Sierra Nevada and the Pyrenees, Intl Journal of Climatology, 44, 2897–2920, https://doi.org/10.1002/joc.8487, 2024.

725 Skamarock, W. C., Klemp, J. B., Dudhia, J., Gill, D. O., Liu, Z., Berner, J., Wang, W., Powers, J. G., Duda, M. G., Barker, D. M., and Huang, X.-Y.: A Description of the Advanced Research WRF Model Version 4.3, UCAR/NCAR, https://doi.org/10.5065/1DFH-6P97, 2021.

Solano-Farias, F., García-Valdecasas Ojeda, M., Donaire-Montaño, D., Rosa-Cánovas, J. J., Castro-Díez, Y., Esteban-Parra, M. J., and Gámiz-Fortis, S. R.: Assessment of physical schemes for WRF model in convection-permitting mode over southern
730 Iberian Peninsula, Atmospheric Research, 299, 107175, https://doi.org/10.1016/j.atmosres.2023.107175, 2024.

Tapiador, F. J., Navarro, A., García-Ortega, E., Merino, A., Sánchez, J. L., Marcos, C., and Kummerow, C.: The Contribution of Rain Gauges in the Calibration of the IMERG Product: Results from the First Validation over Spain, Journal of Hydrometeorology, 21, 161–182, https://doi.org/10.1175/JHM-D-19-0116.1, 2020.

Verrelle, A., Glinton, M., Bazile, E., Le Moigne, P., Randriamampianina, R., Ridal, M., Berggren, L., Undén, P., Schimanke,
735 S., Mladek, R., and Soci, C.: CERRA-Land sub-daily regional reanalysis data for Europe from 1984 to present, https://doi.org/10.24381/CDS.A7F3CD0B, 2022.

Viterbi, R., Cerrato, C., Bassano, B., Bionda, R., Hardenberg, A., Provenzale, A., and Bogliani, G.: Patterns of biodiversity in the northwestern Italian Alps: a multi-taxa approach, Community Ecology, 14, 18–30, https://doi.org/10.1556/ComEc.14.2013.1.3, 2013.

740   Viviroli, D., Kummu, M., Meybeck, M., Kallio, M., and Wada, Y.: Increasing dependence of lowland populations on mountain water resources, Nat Sustain, 3, 917–928, https://doi.org/10.1038/s41893-020-0559-9, 2020.

Yang, Z.-L., Niu, G.-Y., Mitchell, K. E., Chen, F., Ek, M. B., Barlage, M., Longuevergne, L., Manning, K., Niyogi, D., Tewari, M., and Xia, Y.: The community Noah land surface model with multiparameterization options (Noah-MP): 2. Evaluation over global river basins, J. Geophys. Res., 116, D12110, https://doi.org/10.1029/2010JD015140, 2011.

745